


PAPER • OPEN ACCESS

Acoustoelectric photoresponse of graphene nanoribbons

To cite this article: T Poole and G R Nash 2018 *J. Phys. D: Appl. Phys.* **51** 154001


View the [article online](#) for updates and enhancements.



Instruments for Advanced Science


Contact Hiden Analytical for further details:
W www.HidenAnalytical.com
E info@hiden.co.uk

CLICK TO VIEW our product catalogue




Gas Analysis

- dynamic measurement of reaction gas streams
- catalysis and thermal analysis
- molecular beam studies
- dissolved species probes
- fermentation, environmental and ecological studies




Surface Science

- UHV-TPD
- SIMS
- end point detection in ion beam etch
- elemental imaging - surface mapping



Plasma Diagnostics

- plasma source characterization
- etch and deposition process reaction kinetic studies
- analysis of neutral and radical species



Vacuum Analysis

- partial pressure measurement and control of process gases
- reactive sputter process control
- vacuum diagnostics
- vacuum coating process monitoring

Acoustoelectric photoresponse of graphene nanoribbons

T Poole and G R Nash 

College of Engineering, Mathematics and Physical Sciences, University of Exeter, Exeter, EX4 4QF, United Kingdom

E-mail: g.r.nash@exeter.ac.uk

Received 3 December 2017, revised 18 February 2018

Accepted for publication 5 March 2018

Published 20 March 2018



Abstract

The acoustoelectric current in graphene nanoribbons, with widths ranging between 350 nm and 600 nm, has been investigated as a function of illumination. For all nanoribbon widths, the acoustoelectric current was observed to decrease on illumination, in contrast to the increase in acoustoelectric current measured in unpatterned graphene sheet devices. This is thought to be due to the higher initial conductivities of the nanoribbons compared to unpatterned devices.

Keywords: graphene, surface acoustic wave, nanoribbon, acoustoelectric

(Some figures may appear in colour only in the online journal)

1. Introduction

2D materials [1], such as graphene and molybdenum disulphide, naturally lend themselves to integration with surface acoustic wave (SAW) devices. The electric fields associated with a SAW propagating on a piezoelectric substrate can be used to transport charge carriers in these materials, at the speed of sound, over macroscopic distances. This leads to an acoustoelectric (AE) current, an effect that has been extensively studied in other nanostructures [2, 3] for applications such as metrology [4–6] and quantum information [7–13]. AE currents have been measured in both uncoated [14–16] and coated [17, 18] graphene devices, and also in molybdenum disulphide [19]. We have also have previously studied the AE response of large-area graphene sheets produced by chemical vapour deposition (CVD) transferred to LiNbO₃ SAW devices at room temperature [20], low temperature [21], and under illumination [22]. There have also been experimental [23] and theoretical studies [24, 25] of the use of external fields applied to the carrier system amplify the acoustic waves.

One of the unique electronic properties of graphene, the ability to tune its conductivity over orders of magnitude, also allows the AE current to be tuned dynamically [26–30], where

the ambipolar nature of graphene allows the sign of the AE current to be reversed [26–29]. In addition, using an ion gel gate to modulate the conductivity of graphene, Bandhu and Nash [30] not only reversed the direction of the current, but also demonstrated that graphene can be used to control the SAW amplitude and velocity. Optimization of this approach could lead to a practical, cost-effective voltage-controlled velocity shifter suitable for use in wireless sensor applications [30].

We have recently investigated the AE effect in graphene nanoribbons (GNRs) [31], and showed that an AE current can be generated in GNRs with physical widths as small as 200 nm at room temperature (note that the ribbons studied in this work are much larger than those in which a bandgap can be created [32]). The positive current in the direction of the SAWs, which corresponds to the transportation of holes, exhibited a linear dependence on SAW intensity and frequency. This is consistent with the interaction between the charge carriers in the GNRs and the piezoelectric fields associated with the SAWs being described by a relatively simple classical relaxation model. Somewhat counter-intuitively, as the GNR width is decreased, the measured AE current increases. This was thought to be caused by an increase of the carrier mobility due to increased doping arising from damage to the GNR edges. In this paper, we study the effect of illumination on GNRs, and show that the ribbons of widths of 350 nm to 650 nm show a clear photoresponse in the AE current.



Original content from this work may be used under the terms of the [Creative Commons Attribution 3.0 licence](https://creativecommons.org/licenses/by/3.0/). Any further distribution of this work must maintain attribution to the author(s) and the title of the work, journal citation and DOI.

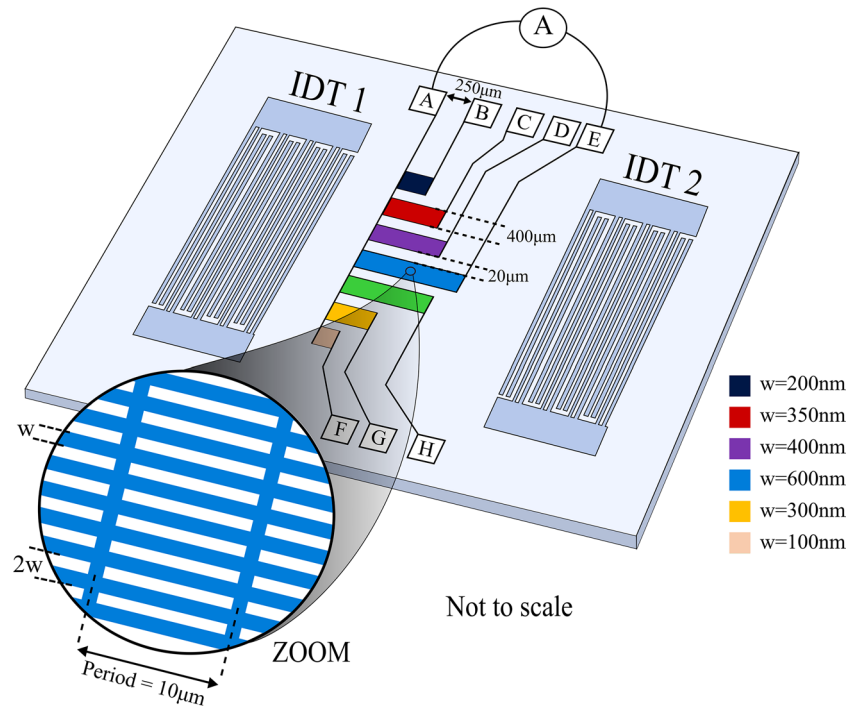


Figure 1. Schematic diagram of the device layout. The magnified region shows how each array is made up of many individual nanoribbons and how a perpendicular bridge structure, patterned into the graphene, is used to maintain electrical conductivity.

2. Method

To study the AE photoresponse of GNRs monolayer graphene, grown by CVD on $\sim 5\text{ mm} \times \sim 5\text{ mm}$ copper foils (Graphene Supermarket), was transferred between the opposing interdigital transducers (IDTs) of a commercially available 128° YX LiNbO_3 SAW delay line with a centre-to-centre IDT separation distance of 5.4 mm, and IDT aperture of 3.25 mm. The IDTs had a double-digit geometry, allowing the efficient excitation of SAWs at a number of resonant frequencies. The graphene was patterned into arrays of parallel nanoribbons with a 50% fill factor, using electron beam lithography and reactive ion etching, with the GNRs oriented such that their long-axis was parallel to the SAW propagation direction. Note that each array consists of many hundreds of nanoribbons, and that individual nanoribbons within an array are connected by a 500 nm-wide perpendicular bridge of graphene every $10\ \mu\text{m}$ to help maintain electrical conductivity [33], as shown schematically in the magnified region of figure 1. To enable the channel width dependence of the AE photoresponse to be studied, neighbouring arrays of GNRs with different nanoribbon widths were fabricated on the same SAW device, as shown schematically in figure 1. This device geometry enables a better comparison of the electronic properties of the GNR arrays, since each nanoribbon experiences the same SAW intensity and has undergone an identical fabrication process. Nanoribbon widths of 350, 400, 500 and 600 nm were characterised, with measured sheet resistances of 3.7, 3.8, 5.4, and $7.0\text{ k}\Omega/\square$ respectively [31], so that the widest ribbons have the smallest electrical conductivity. Further details of the device layout and fabrication process can be found in [31].

All measurements were made under vacuum (chamber pressure approximately 6×10^{-6} mbar) with continuous

pumping to reduce the accumulation of dopants, at room temperature. Continuous wave SAWs were excited at the input transducer using a Hewlett-Packard 8648C RF signal generator, with the RF power set to +20.0 dBm. The AE current, I_{ae} , was measured using a Keithley K2400 source-measurement unit. Two-terminal current-voltage measurements were used to determine the GNR array conductivities, and arrays that were not being characterised were electrically grounded to reduce interference. The SAW amplitude at the output IDT was measured using a LeCroy WaveRunner 204Xi-A digital oscilloscope, and used to estimate SAW intensity.

A Thorlabs MCWHL2 LED (peak emission wavelength of 450 nm) was used to study the AE photoresponse. LED drive currents of 0.2 A and 1.4 A were used, producing an incident light intensity on the sample of 0.24 mW mm^{-2} and 1.20 mW mm^{-2} respectively after correcting for the measurement geometry. A motorised shutter was used to control the exposure of the sample to the LED.

3. Results and discussion

The measured AE current, for a nanoribbon width of 500 nm, is plotted as a function of time for SAW frequencies of 33 MHz and 355 MHz in figures 2(a) and (b) respectively. The vertical dashed lines indicate the time at which the motorised shutter was opened after 1 h, allowing illumination by the LED (with an intensity of 1.20 mW mm^{-2}) for a period of 1 h, before the shutter was then closed again. Although only results from 500 nm wide nanoribbons are presented here, similar results were obtained in all the nanoribbons. A negative current in the direction of SAW propagation was observed in all, corresponding to n-type doping of the nanoribbons, in contrast to the p-doping observed previously in these

nanoribbon arrays [31]. This most likely reflects the increased vacuum pump-out time before these new measurements were undertaken, leading to the removal of surface adsorbates that p-dope graphene, such as molecular water. The magnitude of the AE current was largest for a SAW frequency of 355 MHz in each nanoribbon array. This is thought to arise from an enhanced piezoelectric interaction between the GNRs and the SAWs when the SAW wavelength (approximately 11 μm at 355 MHz) is equal to the periodicity (10 μm) of the perpendicular graphene bridges in the array [31].

Upon illumination, a rapid decrease in the magnitude of the AE current was observed at both SAW frequencies in all GNR arrays. The fast initial change in the current is followed by a much slower decrease in current over the timescale of an hour or so. This effect was also observed in unpatterned graphene [22] and is broadly the same for different SAW frequencies. Unfortunately, the origin of this slow relaxation is unknown, and will be explored in future work. Closing the shutter again causes the current to quickly approach its original value. The *decrease* in the measured AE current under illumination contrasts with the AE photoresponse of continuous graphene sheets [22], where the magnitude of the current *increased* upon exposure to light. A larger change in AE current due to illumination was measured at the higher incident light intensity, and at the higher SAW frequency, as seen previously in graphene sheets. The conductivity of the GNRs (σ^{2D}) was also recorded as a function of time and is plotted as the solid blue line in figure 2(c) for an illumination intensity of 1.20 mW mm^{-2} . Upon exposure to the light, the conductivity quickly decreases, by as much as ~5% in the case of the array of 600 nm-wide GNRs. This compares to a decrease of up to 6% measured in the conductivity of an unpatterned graphene sample under the same illumination [22]. When the shutter is closed, the conductivity increases again towards its value prior to illumination.

The decrease in conductivity under illumination gives rise to an increase in the SAW attenuation per unit length, which can be calculated from the conductivity utilising the classical relaxation model widely used to describe the AE interaction between the SAWs and charge carriers in low dimensional systems [34, 35]:

$$\Gamma = K^2 \frac{\pi}{\lambda} \left[\frac{(\sigma^{2D}/\sigma_M)}{1 + (\sigma^{2D}/\sigma_M)^2} \right] \quad (1)$$

where K^2 is the piezoelectric coupling coefficient (0.056 in 128° YX LiNbO₃), λ is the SAW wavelength, and the attenuation is maximum at a characteristic conductivity, σ_M . In this work, a value of $\sigma_M = 10^{-7} \Omega^{-1}$ was taken, which was extracted from previous measurements where we used an ion gel top gate [30] to modify the conductivity of unpatterned graphene on lithium niobate. The characteristic conductivity σ_M was extracted from the measurement of SAW attenuation as a function of gate bias, with the value of σ_M taken as the value of σ^{2D} when the SAW attenuation was at a maximum (equation (1)). This value is likely to be sensitive to any non-uniformity of the graphene [30], and could vary from sample to sample due to differences in doping. However, as σ^{2D} is

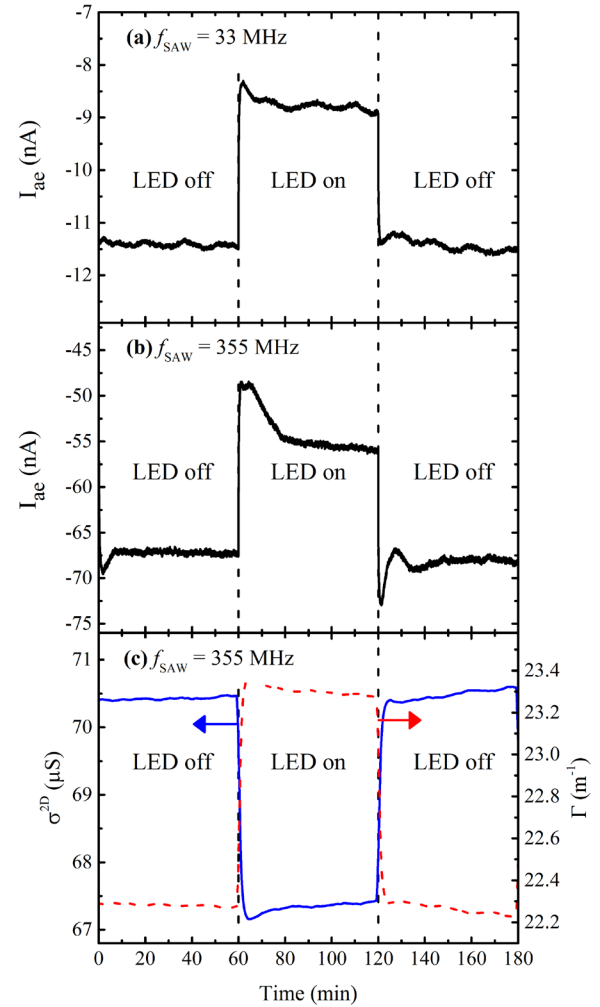


Figure 2. AE current as a function of time at SAW frequencies of (a) 33 MHz and (b) 355 MHz, periodically illuminated by a Thorlabs MCWHL2 LED. (c) The sample conductivity recorded as a function of time (solid blue line). The dashed red line shows the corresponding attenuation coefficient, which was calculated from the measured conductivity using equation (1).

much, much greater than σ_M , for all the ribbon widths and in unpatterned graphene, small variations in the characteristic conductivity are unlikely to alter the interpretation of the results obtained here. Future work will include the simultaneous measurement of the SAW attenuation, as a function of illumination, to probe this further.

The calculated attenuation coefficient is plotted for 500 nm ribbons in figure 2(c), showing how a decrease in conductivity under illumination leads to an increase in the attenuation coefficient. In figure 3(a) the decrease in measured conductivity under illumination, for intensities 0.24 mW mm^{-2} and 1.20 mW mm^{-2} , is plotted as a function of nanoribbon width. A similar trend is observed for both illumination levels, with the largest change in conductivity observed for the widest ribbons. In figure 3(b), the corresponding change in attenuation coefficient, calculated from the measured conductivity using equation (1) is plotted as a function of nanoribbon width, for a SAW frequency of 355 MHz and illumination intensity of 1.20 mW mm^{-2} . The largest change in attenuation coefficient under illumination

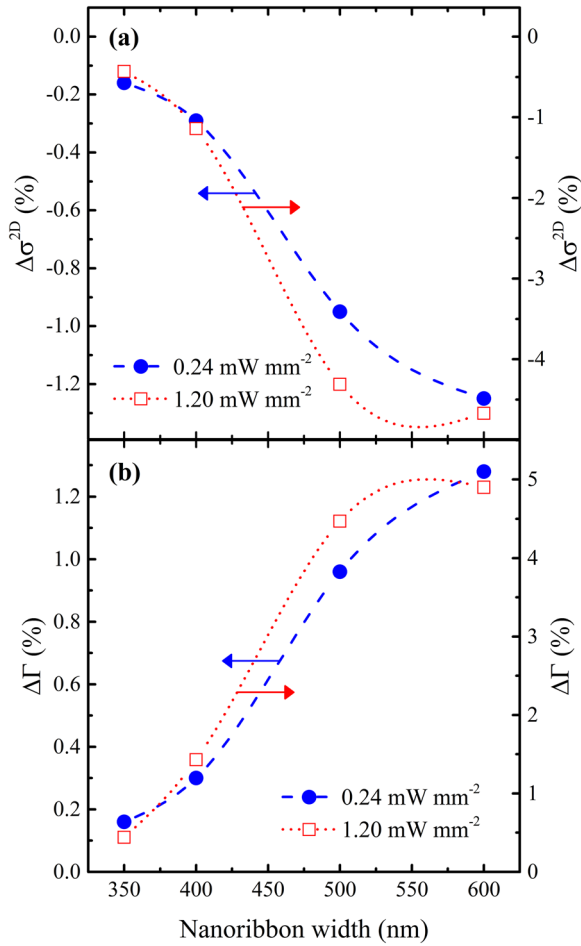


Figure 3. (a) Measured change in conductivity as a function of nanoribbon width for illumination intensities of 0.24 and 1.20 mW mm⁻², (b) calculated, using equation (1), change in attenuation coefficient for the same illumination intensities.

occurs in the widest ribbons. We believe that this is because the widest ribbons have the smallest initial conductivity [31].

The AE current density, j , is determined both by the attenuation, but also by the charge carrier mobility μ :

$$j = -\mu \frac{I\Gamma}{v} \quad (2)$$

where I is the SAW intensity and v is the velocity of the SAW (3979 m s⁻¹ in 128° YX LiNbO₃). In unpatterned graphene sheets, the increase in AE current under illumination was attributed to the generation of a hot carrier distribution [22]. Although this hot carrier distribution leads to a decrease in the charge carrier mobility μ , the corresponding decrease in conductivity led to a much larger increase in the attenuation coefficient, due to the non-monotonic behaviour described by equation (1), resulting in an overall increase in the measured AE current.

The contrasting *decrease* of the measured AE current, under illumination, of the nanoribbons studied here is therefore likely due to the large difference in the initial conductivity of the unpatterned and nanoribbon graphene. The arrays of the 600 nm-wide and 350 nm-wide GNRs have conductivities $\sim 11\times$ and $21\times$ greater [31] respectively than

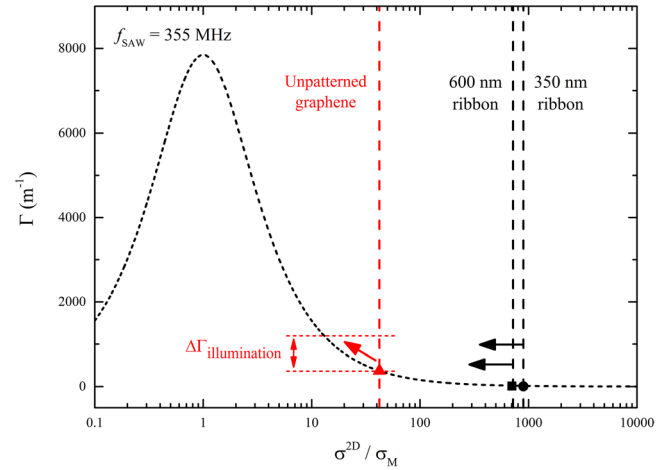


Figure 4. Calculated attenuation coefficient, Γ , as a function of conductivity normalised to the characteristic conductivity σ_M , is shown by the black dotted line for $f_{SAW} = 355$ MHz. The attenuation coefficient calculated for unpatterned graphene (red triangle) and 600 nm (black square) and 350 nm (black circle) wide ribbons are also shown. Arrows indicate the change in conductivity of these structures when illuminated, and the red dotted horizontal lines indicate the size of the associated change in attenuation coefficient for unpatterned graphene.

that of a typical unpatterned device [20–22]. Therefore, a decrease in the conductivity of the nanoribbons under illumination leads to a smaller change in the attenuation coefficient than that seen in the continuous graphene. This is shown schematically in figure 4, where the calculated attenuation coefficient (equation (1)) is plotted as a function of (σ^{2D} / σ_M) . Under illumination, the conductivity of the nanoribbons decreases, but this only leads to a relatively small increase in the attenuation coefficient as compared to that observed in unpatterned graphene. This relatively small increase in the attenuation coefficient cannot therefore be large enough to compensate for the decrease in mobility, which overall leads to a decrease in the AE current under illumination.

4. Conclusion

In conclusion, we have investigated the AE current in arrays of monolayer CVD GNRs with widths in the range 350–600 nm, as a function of illumination. Under illumination, both the AE current and the conductivity were observed to decrease, where the decrease in conductivity is consistent with the generation of a hot carrier distribution. The decrease in AE current contrasts with the increase in current observed in unpatterned graphene devices under illumination, even though the conductivity of these devices was also observed to decrease under illumination. This difference in observed behaviour is thought to be due to the very high conductivity of the nanoribbons compared to unpatterned graphene. A decrease of the conductivity of the ribbons under illumination only therefore leads to a small increase in the attenuation coefficient of the SAW, and is not enough to compensate for the reduction in mobility due to increased carrier–carrier scattering. Overall, the AE current therefore decreases on illumination.

Acknowledgments

GRN acknowledges the support of the UK Engineering and Physical Sciences Research Council through a Fellowship in Frontier Manufacturing (Grant No. EP/J018651/1). The authors would like to thank Faye Langston for help with drafting figure 1.

ORCID iDs

G R Nash  <https://orcid.org/0000-0002-5321-4163>

References

- [1] Mas-Balleste R, Gomez-Navarro C, Gomez-Herrero J and Zamora F 2011 2D materials: to graphene and beyond *Nanoscale* **3** 20–30
- [2] Rotter M, Wixforth A, Ruile W, Bernklau D and Riechert H 1998 Giant acoustoelectric effect in GaAs/LiNbO₃ hybrids *Appl. Phys. Lett.* **73** 2128–30
- [3] Fal'ko V I, Meshkov S V and Iordanskii S V 1993 Acoustoelectric drag effect in the two-dimensional electron gas at strong magnetic field *Phys. Rev. B* **47** 9910–2
- [4] Shilton J M, Mace D R, Talyanskii V I, Galperin Y, Simmons M Y, Pepper M and Ritchie D A 1996 High-frequency single-electron transport in a quasi-one-dimensional GaAs channel induced by surface acoustic waves *J. Phys.: Condens. Matter* **8** L337–43
- [5] Fletcher N E, Ebbecke J, Janssen T J B M, Ahlers F J, Pepper M, Beere H E and Ritchie D A 2003 Quantized acoustoelectric current transport through a static quantum dot using a surface acoustic wave *Phys. Rev. B* **68** 245310
- [6] Ford C J B 2017 Transporting and manipulating single electrons in surface-acoustic-wave minima *Phys. Status Solidi b* **254** 1600658
- [7] Barnes C H W, Shilton J M and Robinson A M 2000 Quantum computation using electrons trapped by surface acoustic waves *Phys. Rev. B* **62** 8410–9
- [8] Foden C L, Talyanskii V I, Milburn G J, Leadbeater M L and Pepper M 2000 High-frequency acousto-electric single-photon source *Phys. Rev. A* **62** 011803
- [9] Gumbs G and Abranyos Y 2004 Quantum entanglement for acoustic spintronics *Phys. Rev. A* **70** 050302
- [10] Giavaras G, Jefferson J H, Ramšak A, Spiller T P and Lambert C J 2006 Quantum entanglement generation with surface acoustic waves *Phys. Rev. B* **74** 195341
- [11] Smith S J, Nash G R, Lewis M F, Bartlett C J, Buckle L, Emeny M T and Ashley T 2007 Acoustic charge transport in lateral n-i-p InSb/Al_xIn_{1-x}Sb quantum well diodes *AIP Conf. Proc.* **893** 1111–2
- [12] Couto O D D Jr, Lazić S, Iikawa F, Stotz J A H, Jahn U, Hey R and Santos P V 2009 Photon anti-bunching in acoustically pumped quantum dots *Nat. Photon.* **3** 645–8
- [13] Hermelin S, Takada S, Yamamoto M, Tarucha S, Wieck A D, Saminadayar L, Bauerle C and Meunier T 2011 Electrons surfing on a sound wave as a platform for quantum optics with flying electrons *Nature* **477** 435–8
- [14] Miseikis V, Cunningham J E, Saeed K, O'Rourke R and Davies A G 2012 Acoustically induced current flow in graphene *Appl. Phys. Lett.* **100** 133105
- [15] Santos P V, Schumann T, Oliveira M H Jr, Lopes J M J and Riechert H 2013 Acousto-electric transport in epitaxial monolayer graphene on SiC *Appl. Phys. Lett.* **102** 221907
- [16] Roshchupkin D *et al* 2015 Surface acoustic wave propagation in graphene film *J. Appl. Phys.* **118** 104901
- [17] Hernandez-Minguez A, Tahraoui A, Lopes J M J and Santos P V 2016 Acoustoelectric transport at gigahertz frequencies in coated epitaxial graphene *Appl. Phys. Lett.* **108** 193502
- [18] Liou Y-T, Hernández-Minguez A, Herfort J, Lopes J M J, Tahraoui A and Santos P V 2017 Acousto-electric transport in MgO/ZnO-covered graphene on SiC *J. Phys. D: Appl. Phys.* **50** 464008
- [19] Preciado E *et al* 2015 Scalable fabrication of a hybrid field-effect and acousto-electric device by direct growth of monolayer MoS₂/LiNbO₃ *Nat. Commun.* **6** 8593
- [20] Bandhu L, Lawton L M and Nash G R 2013 Macroscopic acoustoelectric charge transport in graphene *Appl. Phys. Lett.* **103** 133101
- [21] Bandhu L and Nash G R 2014 Temperature dependence of the acoustoelectric current in graphene *Appl. Phys. Lett.* **105** 263106
- [22] Poole T, Bandhu L and Nash G R 2015 Acoustoelectric photoresponse in graphene *Appl. Phys. Lett.* **106** 133107
- [23] Insepov Z, Emelin E, Kononenko O, Roshchupkin D V, Tnyshytkbayev K B and Baigarin K A 2015 Surface acoustic wave amplification by direct current-voltage supplied to graphene film *Appl. Phys. Lett.* **106** 023505
- [24] Yurchenko S O, Komarov K A and Pustovoi V I 2015 Multilayer-graphene-based amplifier of surface acoustic waves *AIP Adv.* **5** 057144
- [25] Dompok K A, Mensah S Y, Abukari S S, Sam F and Mensah N G 2016 Amplification of acoustic waves in armchair graphene nanoribbon in the presence of external electric and magnetic fields *Physica E* **83** 420–5
- [26] Okuda S, Ikuta T, Kanai Y, Ono T, Ogawa S, Fujisawa D, Shimatani M, Inoue K, Maehashi K and Matsumoto K 2016 Acoustic carrier transportation induced by surface acoustic waves in graphene solution *Appl. Phys. Express* **9** 045104
- [27] Zheng S, Zhang H, Feng Z, Yu Y, Zhang R, Sun C, Liu J, Duan X, Pang W and Zhang D 2016 Acoustic charge transport induced by the surface acoustic wave in chemical doped graphene *Appl. Phys. Lett.* **109** 183110
- [28] Tang C-C, Chen Y-F, Ling D C, Chi C C and Chen J-C 2017 Ultra-low acoustoelectric attenuation in graphene *J. Appl. Phys.* **121** 124505
- [29] Liang J, Yang X, Zheng S, Sun C, Zhang M, Zhang H, Zhang D and Pang W 2017 Modulation of acousto-electric current using a hybrid on-chip AlN SAW/GFET device *Appl. Phys. Lett.* **110** 243504
- [30] Bandhu L and Nash G R 2016 Controlling the properties of surface acoustic waves using graphene *Nano Res.* **9** 685–91
- [31] Poole T and Nash G R 2017 Acoustoelectric current in graphene nanoribbons *Sci. Rep.* **7** 1767
- [32] Celis A, Nair M N, Taleb-Ibrahimi A, Conrad A H, Berger C, de Heer W A and Tejeeda A 2016 Graphene nanoribbons: fabrication, properties and devices *J. Phys. D: Appl. Phys.* **49** 143001
- [33] Luxmoore I J, Gan C H, Liu P Q, Valmorra F, Li P, Faist J and Nash G R 2014 Strong coupling in the far-infrared between graphene plasmons and the surface optical phonons of silicon dioxide *ACS Photonics* **1** 1151–5
- [34] Wixforth A, Scriba J, Wassermeier M, Kotthaus J P, Weimann G and Schlapp W 1989 Surface acoustic waves on GaAs/Al_xGa_{1-x} heterostructures *Phys. Rev. B* **40** 7874–87
- [35] Nash G R, Bending S J, Boero M, Grambow P, Eber K and Kershaw Y 1996 Anisotropic surface acoustic wave scattering in quantum-wire arrays *Phys. Rev. B* **54** R8337–40